Biochimica et Biophysica Acta 1848 (2015) 2138–2153

Contents lists available at ScienceDirect

Biochimica et Biophysica Acta

journal homepage: www.elsevier.com/locate/bbamem

Spatial profiles of potential, ion concentration and flux in short unipolar and bipolar nanopores

Mohammad Tajparast [a], Gautam Virdi [b], Mladen I. Glavinović [c,*]

[a] Department of Civil Engineering and Applied Mechanics, McGill University, Montreal, QC, Canada
[b] Department of Mechanical Engineering, McGill University, Montreal, QC, Canada
[c] Department of Physiology, McGill University, Montreal, QC, Canada

ARTICLE INFO

Article history:
Received 17 September 2014
Received in revised form 13 May 2015
Accepted 29 May 2015
Available online 14 June 2015

Keywords:
Fusion pore flicker
Rectification
Poisson–Nernst–Planck
Ion fluxes
Engineered nanopores

ABSTRACT

During release of vesicular content the resistance of the fusion pore sometimes changes rapidly and repeatedly. However, it is not clear why the pore 'flickers'. Engineered nanopores often rectify, but how different factors influence the rectification requires clarification. To better understand the ionic 'causes' of pore conductivity and its changes we simulated ion transport through a short nanopore using Poisson–Nernst–Planck equations, coupling it to the transport of water using Navier–Stokes equations. We extracted the potential, concentration, and ion flux profiles. In uniformly charged nanopores the voltage bias determines which counter-ion flux dominates, and it is carried by the counter-ions of the highest concentration. In unipolar nanopores this simple rule breaks down. The dominant counter-ion in the charged half is from the adjacent compartment, but the bias determines what counter-ion flux is dominant — the same ion (regular bias), or a different and smaller (reverse bias), and this difference determines the level of rectification. In bipolar nanopores the dominant counter-ions in each half are from the adjacent compartments, and the total ion concentration dips in the middle near the wall. With regular bias the total ion concentration peaks in the pore center; the ions that carry the current through the nanopore start as counter-ions and their fluxes are large. With reverse bias the total concentration dips near the wall and in the center, both dominant ion fluxes through the nanopore start as co-ions and are very small, whereas those starting as counter-ions do not go through.

1. Introduction

Control of ion flow through ion channels and regulation of ion selectivity are very important in biology as they influence the functioning of many biological processes [1]. Fusion pores – another type of biological nanopore – provide a passage for the release of vesicular content [2]. During secretion of their content – molecules (transmitters, hormones, peptides) and ions – the resistance of fusion pores sometimes changes rapidly and repeatedly, i.e., they 'flicker' [3]. The origin of this 'flicker' is not clear. To what extent the 'flicker' of the fusion pore is due to the rapidly changing pore radius, or due to changing intra-vesicular concentration of ions or transmitter, or due to change in the fusion pore wall fixed charge density is not known. The presence of 'flicker' would alter the amount of the transmitter or hormone released and thus the presynaptic quantal size. This would in turn determine the response to the transmitter released from a single vesicle; [4,5]. To fully understand this problem it is necessary to evaluate the conductivity of the nanopores under a variety of conditions and what factors influence it. Whereas the measurements of the conductance of nanopores such as biological ion channels (or fusion pores) are simple, the mechanisms involved in determining their conductivity are quite complex and are still poorly understood [6].

Nanopores with subnanometer radius, differing in shape and with chosen surface charge density and distribution, can now be manufactured using modern nanofabrication techniques [7]. Such engineered nanopores have many useful applications [8]. One of the most useful applications of such nanopores is as rectifiers, i.e., as devices that have asymmetric current–voltage characteristics [9]. The rectifying nanopores resemble semiconductor diodes [10] and can be used as components of ionic circuits to switch and re-direct the flow of ions. Indeed, the nanopores with the characteristics of diodes have been used recently to create ionic logic gates [11,12]. In ionic transistor type devices the charge is carried by ions (or generally charged molecules) [13], and ion mobility is well below that of the holes and electrons in conventional semiconductor transistors. However, they transmit not only charges, but also chemical information that is variable and can be highly specific, and can regulate and control different chemical and biological processes [14]. Unipolar nanopores (where one half of the nanopore is uniformly charged, and another half is neutral) may be used as nanofluidic diodes. However, devices with uniformly charged zones with the same charge density of opposite polarity are the most promising as highly performing diodes. For one voltage polarity these bipolar diodes can have

* Corresponding author at: Department of Physiology, McGill University, 3655 Sir William Osler Promenade, Montreal, QC H3G 1Y6, Canada.
E-mail address: mladen.glavinovic@mcgill.ca (M.I. Glavinović).

http://dx.doi.org/10.1016/j.bbamem.2015.05.023
0005-2736/

currents that are much (>100 times) higher than those having the opposite voltage polarity [15–17].

What causes rectification? It has been argued that rectification occurs because ions can enter into the nanopore to produce a steady flow of current if the bias is regular, but with reverse bias they move out of the pore and cannot be replenished resulting in a current that is very small [10]. For rectification to be observed all ions need to interact with the charges on the wall requiring the pore radius to be sufficiently small. Rectification also depends on the length of the nanopore. In unipolar diode the depletion zone (the region with low ionic concentrations) is formed in the neutral zone, which thus needs to be sufficiently long for significant rectification to be observed [18]. In contrast, the depletion zone in bipolar diodes exists between regions with positive and negative surface charges, which limits less our ability to shrink longitudinally the nanopore. The bias should also influence the conductivity–radius (and thus the rectification–radius) relationship in short unipolar and bipolar nanopores. If the bias is regular the conductivity of the nanopore will be high, it will decrease if the pore widens, but if it is low (reverse bias) it will increase greatly with pore widening. We expect that the conductivity is typically nonuniform within the nanopore (unipolar or bipolar). However, is the conductivity not just within the depletion layer, but throughout bipolar nanopore, very low if the bias is reverse?Finally, does the rectification of bipolar nanopores increase not only if it becomes narrower, but also if the charge density on the wall increases [19]? To better understand the mechanisms determining pore conductivity and rectification we look into how ionic fluxes and their spatial distribution are affected as rectification changes.

We simulated the transport of K^+, glutamate$^-$, Na^+ and Cl^- through a nanopore using the Poisson–Nernst–Planck equation. This was coupled to the transport of water using the Navier–Stokes equations [19,20]. The computational domain consists of a charged, narrow (r = 1–4 nm) and short (L = 10 nm) cylindrical nanopore flanked by two compartments, one representing the intra-cellular (or intra-vesicular) space, and another the extra-cellular space, which are separated by the membrane. In such a nanopore the interactions of ions with the charges on the wall are as a rule strong. Between two compartments there are concentration, potential and pressure gradients. The concentrations of ions in two compartments flanking the nanopore (K^+ and glutamate$^-$ or Glu^- in the upper compartment, and Na^+ and Cl^- in the lower compartment) are the same, but their diffusion constants differ.

2. Methods

2.1. Mathematical model

The Poisson–Nernst–Planck (PNP) equations (composed of the Poisson (1) and Nernst–Planck (3) equations) were used to calculate ionic fluxes within and outside of the nanopore. The Poisson equation evaluates the electrostatic potential (Φ):

$$-\nabla.\varepsilon_0\varepsilon_r\nabla\Phi = \rho_e \tag{1}$$

where ε_0 gives the permittivity of vacuum, ε_r stands for relative permittivity of solution, and ∇ is the gradient operator. The charge density ρ_e is calculated as follows:

$$\rho_e = F\sum z_a c_a \left(= e\sum z_a n_a\right). \tag{2}$$

F stands for Faraday constant (9.648×10^4 C/mol), z_a denotes the valence of ion a, c_a accounts for the molar concentration of ion a [mol/m^3], n_a is the number density of ion a. Note that International System of Units are used in these simulations, and mol/m^3 translates to mmol/l (or simply mM). The factors that also impact the potential within the simulation space are the fixed charges on the wall, the mobile charges in the solution and the potential at the controlling edges.

The Nernst–Planck equation describes the movement (by convection–diffusion–migration) of ions in the solution:

$$\mathbf{J_a} = \mathbf{u}c_a - D_a\nabla c_a - m_a z_a F^a c_a \nabla\Phi \tag{3}$$

where $\mathbf{J_a}$, D_a, and m_a stand for molar flux [mol/(m^{2}s)], diffusivity, and mobility of ion a ($m_a = D_a/(RT)$), respectively; $\mathbf{u}$ accounts for fluid velocity, while F, R and T are Faraday constant, gas constant [8.31 J/(mol · K)], and absolute temperature (in Kelvin), respectively. The following equation accounts for the conservation of ionic mass at steady state:

$$\nabla.\mathbf{J_a} = 0. \tag{4}$$

The following expression defines the divergence operator in the cylindrical coordinate system:

$$\nabla.\mathbf{J} = \frac{1}{r}\frac{\partial}{\partial r}(rJ_r) + \frac{\partial J_z}{\partial z} \tag{5}$$

where J_r and J_z are the r- and z-components of vector $\mathbf{J}$.

The fluid velocity $\mathbf{u}$ that drives the convective movement of ions in the solution is estimated using the Navier–Stokes (NS) equations at the steady state as follows:

$$\rho_f(\mathbf{u}.\nabla\mathbf{u}) = -\nabla p + \nabla.\left[\mu\left[\nabla\mathbf{u} + (\nabla\mathbf{u})^T\right]\right] + \mathbf{F_e} \tag{6}$$

$$\nabla.\mathbf{u} = 0. \tag{7}$$

The conservation of momentum is given by Eq. (6), whereas the mass conservation is described through Eq. (7). $\mathbf{F_e}$ stands for the electric force per unit volume ($\mathbf{F_e} = -\rho_f\nabla\Phi$). In the equations given above ρ_f, μ, and p denote the density, viscosity, and pressure of the fluid respectively.

2.2. Geometry of simulation domain, parameters and boundary conditions

Fig. 1A depicts the simulation domain comprising the cylindrical nanopore, piece of the membrane, and two compartments on two sides of the nanopore indicating an intracellular (or intra-vesicular) space and an extra-cellular (or extra-vesicular) space. The total length of the simulation space was 30 nm, and the length of the nanopore (L) and of both compartments representing the vesicular and extracellular spaces were 10 nm each. The nanopore radius R ranged from 1.0 to 4.0 nm, whereas the radius W of the compartments representing the vesicular and extracellular spaces was 11.0 nm.

The boundaries are enumerated in Fig. 1B, and Table 1 lists the boundary conditions for electro-statics, electrokinetics and fluidics. In this study we consider that glutamate is negatively charged, with a single negative charge, which remains constant throughout simulations (the glutamate is thus considered as an anion, and. the complexities of the shape of this molecule are ignored). We also assume that the positive ion in the vesicle is potassium. The sodium would have been a physiologically better choice, but we chose potassium to distinguish it from sodium in the extra-cellular compartment. It should also be noted that the surface charge density (σ) on the internal wall of the nanopore (boundary 5) including the curved parts at both ends (boundary 5) of 64 mC/m^2 is equivalent to 30.8 unitary charges for a 1.0 nm radius nanopore (or 114.6 unitary charges for a 4.0 nm nanopore). These values agree well with the values reported previously for the cell membrane (one elementary negative fixed charge per 1–4 nm^2, which is equal to a charge density of 40–160 C/m^2; [21,22]).

The finite element method was used to evaluate the coupled system of PNP and NS equations. The diffusion constants for ions, transmitters and hormones diffusing in free aqueous solution are known [1,23]. It is less clear what the values may be in the confined space of the nanopore, where the non-electrostatic and electrostatic interactions with its walls [24] will restrict their movement. To simplify the

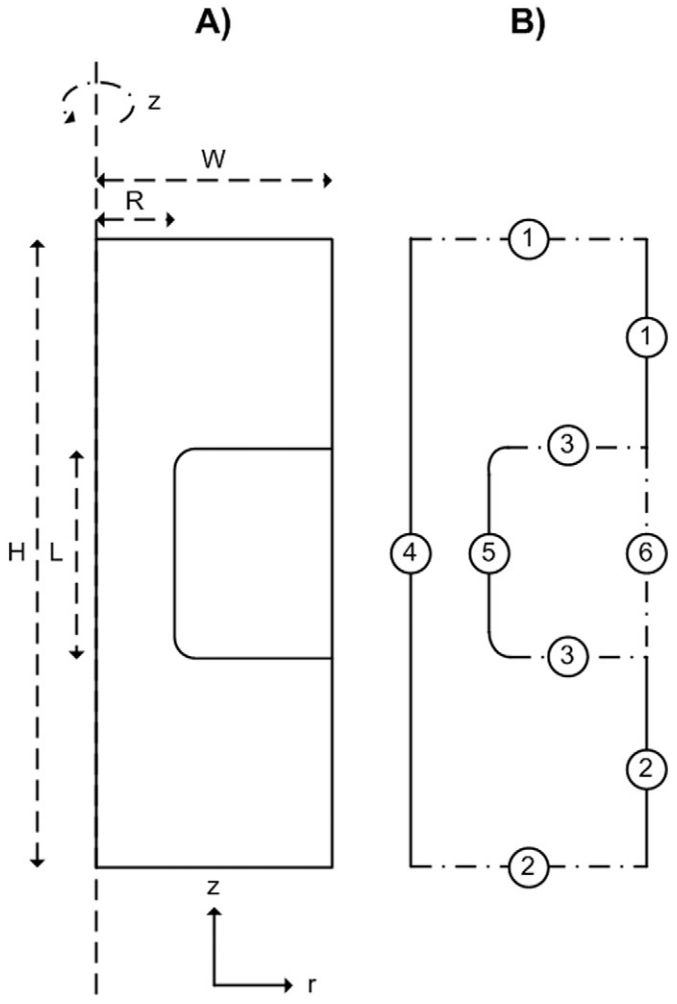

Fig. 1. A) The hemi-section of the simulation space, which includes the cylindrical nanopore, two compartments (one on each side) and the patch of membrane separating them. The rotation of the hemi-section about the central axis by 180° generates the 3D-model. The radius R of the nanopore ranges from 1.0 to 4.0 nm (see Results), and its length L is 10 nm. The radius W of the two compartments flanking the nanopore is 11 nm. The total length of the simulation domain is 30.0 nm. The radii of curvature at the pore entrance and exit are 1.0 nm. B) Axial symmetry condition applies on all variables along the axis of the nanopore (boundary 4). The Nernst–Planck boundary conditions were concentrations of K^+–glutamate$^-$ on two external controlling edges of the upper compartment (boundaries 1) and Na^+–Cl^- on the edges of lower compartment (boundaries 2). At the solution–membrane interface (boundaries 3 and 5) the boundary condition (Nernst–Planck) was insulation/symmetry, and no-slip (Navier–Stokes). The Poisson boundary condition was the surface charge on the internal wall of the nanopore including the curved parts (boundary 5) and on the external wall. All boundary conditions values are shown in Table 1.

computation, we assumed that all diffusion coefficients (but also the dielectric constant and specific viscosity) are spatially uniform, isotropic and the same as in the aqueous solution. The values of all constants and parameters are given in Table 2.

Electrophysiological studies suggest that ion channels and fusion pores are similar [3]. However, whereas an ion channel is known to be formed of well-characterized proteins, the composition of a fusion pore is less clear [25]. If it starts as a protein it becomes progressively more lipidic as the pore dilates. Irrespective of how the fusion pore is envisioned it (like an ion channel) forms a water-filled nanopore controlling the transport of ions and transmitters. The permeation through a nanopore is determined by its geometry, by the permittivity of the pore-forming material, and by the charges on its walls. We make the assumption that the pore is cylindrical. This is a simplifying, but necessary assumption. The permittivity of the pore-forming material is assumed to be low. We take it to be 2, a value that is close to the values reported for lipid membranes and proteins, which are both low [20].

Table 2
Model constants and parameters.

Params	Value	Unit	Description	Refs
e	1.602×10^{-19}	C	Elementary charge	
R	8.314	J/(mol · K)	Universal gas constant	
D_1	1.960×10^{-9}	m^2/s	Diffusion coefficient of K^+ ions	[1]
D_2	0.760×10^{-9}	m^2/s	Diffusion coefficient of glutamate$^-$	[23]
D_3	1.330×10^{-9}	m^2/s	Diffusion coefficient of Na^+ ions	[1]
D_4	2.030×10^{-9}	m^2/s	Diffusion coefficient of Cl^- ions	[1]
D_5	0.790×10^{-9}	m^2/s	Diffusion coefficient of Ca^{2+} ions	[1]
T	300.0	K	Temperature	
μ	1	mPa · sec	Fluid viscosity	[20]
e_0	8.854×10^{-12}	F/m	Permittivity of vacuum	
e_{rw}	80.0	Dimensionless	Relative permittivity of solution	[20]
e_{rm}	2.0 (or 8.0)	Dimensionless	Relative permittivity of membrane	[20]
ρ_m	785.0	kg/m^3	Membrane density	[20]

The charges on the walls of the proteinaceous pore result from the presence of bound ions, amino acid side chains and the carboxy- and amino-termini. However, the charge on amino acid side chains is influenced by the pH of the solution and the pK_A of the side chains. The deprotonated form predominates if the pH is above the pK_A of a group. If so the charge on acidic side chains approaches −1 and on the basic side chains it is near 0. In contrast, the protonated form of the group dominates if the pH is below the pK_A of a group, leaving the acidic side chains with a charge near 0 and the basic side chains with a charge near +1. In lipidic (or partly lipidic) nanopores the charges on the polar heads of the lipids forming the nanopore will also be pH-sensitive. It is thus clear that the charge density on the wall of the fusion pore will be influenced by the pH of the solution in the pore which during secretion will depend on both the intra-vesicular and extra-cellular pH. Given that the interior of a vesicle is acidified prior to release [26], the opening of the fusion pore should lead to a progressively more positively charged pore wall. Note also that as the pore dilates its lipid content may rise. If so, it may become a dominant component of the pore wall. Negative charge on the phosphatidylserine will be present together with positive charges induced by the intra-vesicular low pH. Finally, the pore wall charge density will generally not be uniform, and the degree of non-uniformity will change with time.

2.3. Assumptions of continuum modeling of transmitter and ion transport in nanopores

The classical Poisson–Nernst–Planck equation assumes the ions as infinitesimally small, and ion–water and ion–wall and the ion–ion

Table 1
Boundary conditions.

Boundary	Electrostatics	Electro-kinetics	Fluidics
B1	Electric potential V_u (−80 mV to +80 mV)	K^+–glutamate$^-$ (15 to 150 mM)	Pressure (0 to 500 kPa)
B2	Electric potential V_d (0 mV)	Na^+–Cl^- (15 to 150 mM)	Pressure (0 kPa)
B3	Surface charge density (0 C/m^2)	Insulation symmetry	No-slip and no-penetration
B4	Axial symmetry	Axial symmetry	Axial symmetry
B5	Surface charge density σ_e ($0–64 \times 10^{-3}$ C/m^2)	Insulation symmetry	No-slip and no-penetration
B6	Zero charge	NA	NA

interactions are all considered in a mean-field fashion. Molecular aspects of such interactions are not considered. Moreover, in Navier–Stokes equations the fluid density is assumed not to change significantly over intermolecular distances. However, molecular dynamics simulations have shown that the ion distributions near the channel wall are influenced by the ion–water and ion–wall and interactions, as well as by the finite size and discreteness of the ions and water molecules [24]. These contributions, which may be important for very narrow pores, are considered as being beyond the scope of this study. The simulations in this study are stationary even though the radius of the fusion pore changes. Since the changes of radius are much slower than the ion transport through the nanopore the problem can be considered as quasi-static.

3. Results

3.1. Spatial profiles of potential and ion concentration in uniformly charged nanopores

In order to evaluate how the pore wall charge patterning alters the potential and concentration profiles we first present such profiles in a uniformly charged nanopore. As expected the potential in the nanopore is under strong dual influence of the fixed charges on the pore wall and the voltage bias (Fig. 2A_1–A_2). Given that the pore is narrow (its radius is 1 nm) and that the density of fixed charges on the pore wall is high, the co-ions are almost completely excluded from the nanopore, even in the pore center, where the repulsive interactions with the pore wall charges is the weakest (Fig. 2B_1–B_2 and C_1–C_2). Note that the co-ions are the ions of the same charge (and counter-ions of the opposite charge) as those of the fixed charges on the wall. The counter-ion (Glu^- and Cl^-) concentrations are much higher, especially near the wall (0.05 nm from the wall), owing to the attractive interactions with the pore wall charges, and much higher than the corresponding values in the compartments flanking the nanopore. The concentration levels of counter-ions are elevated (and of co-ions depressed) due to the need to maintain the approximate electrical neutrality of the nanopore [27]. Indeed, the excess concentration (the concentration difference between counter-ions and co-ions) remains almost constant axially near the wall and in the pore center, but its values are lower in the center. Moving downwards Glu^- concentration in the nanopore gradually decreases, whereas the Cl^- concentration increases. Their concentration peaks are near the corresponding entrance of the nanopore (Glu^- peak at the top and Cl^- at the bottom). Out of the nanopore their concentration drops precipitously to the level in the corresponding compartment. Finally, the potential at the upper controlling edges (V_u) determines which of two counter-ions dominates in the nanopore. If V_u is negative (−80 mV) Glu^- dominates, and if it is positive (+80 mV) Cl^- dominates. The potential at the lower controlling edges (V_d) was in both cases 0 mV.

3.2. Spatial profiles of potential and ion concentrations in unipolar nanopores

Fig. 3A_1–A_2 depict the potential profiles within the unipolar nanopore (the lower half was charged with a charge density of +64 mC/m^2). In both cases the V_d was 0 mV, but V_u was −80 mV (reverse bias; left panels) or +80 mV (regular bias; right panels). Greater potential in the charged half of the nanopore is highly localized regardless of bias, but if the bias is regular the potential due to fixed charges is superimposed on a potential at its low end (Fig. 3A_1), whereas with the reverse bias it is superimposed on a potential at its high end (Fig. 3A_2). As a result not only the potential but also the concentration profiles are very different.

If the bias is regular one counter-ion dominates in the charged half of the nanopore and comes from the compartment flanking it (Cl^-). The concentration of other counter-ion (Glu^-) is much lower even near the wall (Fig. 3B_2). However, in the pore center K^+ (co-ion) concentration is significant, whereas the concentrations of Glu^- and Na^+ are low. However, in the uncharged half the concentration of both counter-ions, and of one co-ion (K^+) are all comparatively high. K^+ ions are attracted by the high concentration of Cl^- in the upper half, and by the positive V_u (Fig. 3C_2). If the bias is reverse the concentrations of both counter-ions are comparatively high in the charged half of the nanopore (although Cl^- dominates) and the co-ions are again excluded. However, unlike with regular bias in the uncharged half the concentrations of all ions are suppressed (Fig. 3B_1 and C_1), and this has important implications for the ion flow through the nanopore (see below). Finally, note that whereas with regular bias the total ion concentration in uncharged half is below that in the charged half, but is clearly above that outside of the nanopore, with reverse bias it is below that outside of the nanopore.

3.3. Spatial profiles of potential and ion concentrations in bipolar nanopores

In bipolar nanopores both positive and negative fixed charges are present on the wall. As in unipolar nanopores the potential profiles change rapidly axially and the effect of fixed charges is highly localized (Fig. 4A_1–B_1). However, the potential difference where two halves meet is much greater with reverse bias (Fig. 4A_2). The concentration profiles also differ significantly, especially in the middle. With reverse bias only one type of counter-ion is present in each half of the nanopore (and comes from the adjacent compartment; K^+ in the upper and Cl^- in the lower compartment), and this holds true throughout the nanopore including in the pore center (Fig. 4B_2–B_3). The counter-ions from the compartment that is not adjacent (Na^+ in the upper and Glu^- in the lower compartment) do not enter because of electro-static forces that move them back, and co-ions (Glu^- in the upper half and Na^+ in the lower half) are also excluded. Finally, there are effectively no ions of any kind in the middle of the nanopore. If bias is regular, the total concentration within the nanopore is significantly higher, dips in the middle of the nanopore near the wall but only a little (Fig. 4A_2), and in the pore center it peaks instead (Fig. 4A_3). In each half of the nanopore one counter-ion from the adjacent compartment dominates (K^+ ions in the upper half and Cl^- ions in the lower half), but are confined exclusively to one half of the nanopore, and present also in the other half at comparatively high concentration especially in the pore center. There are however no Glu^- or Na^+ ions in the nanopore. The excess concentration (near the wall and in the pore center) is essentially independent of the voltage bias. Note also that the values are similar to those in the charged half of the unipolar nanopores and in the uniformly charged nanopores. The approximate electrical neutrality is well maintained near the charged parts.

Given that the ion depletion in the middle of the bi-polar nanopore is taken as the cause of the rectification (see Discussion), we quantify such changes for different fixed charge densities. Fig. 5A depicts the axial profiles of the total ion concentration near the wall for four different charge densities. The total ion concentration is high within each oppositely charged half of the nanopore, and low in the middle of the nanopore. The depletion is clearly higher at higher charge densities (Fig. 5B), but the width of the depletion layer (estimated at 50% depletion) is narrower (Fig. 5C). Finally, the concentration minimum diminishes greatly as the charge density rises (Fig. 5D).

3.4. Ion fluxes in uniformly charged nanopores

Given the cylindrical geometry of the nanopore, the ion fluxes can be either axial or radial. The upward (or inward; i.e., from the extra-cellular into intra-vesicular space) axial fluxes are considered as positive, whereas the downward (or outward; i.e., from the intra-vesicular into extra-cellular space) fluxes are considered as negative. Positive radial fluxes are from the center towards the wall, and negative from the wall towards the center. Fig. 6 gives the 2D color plots of axial fluxes

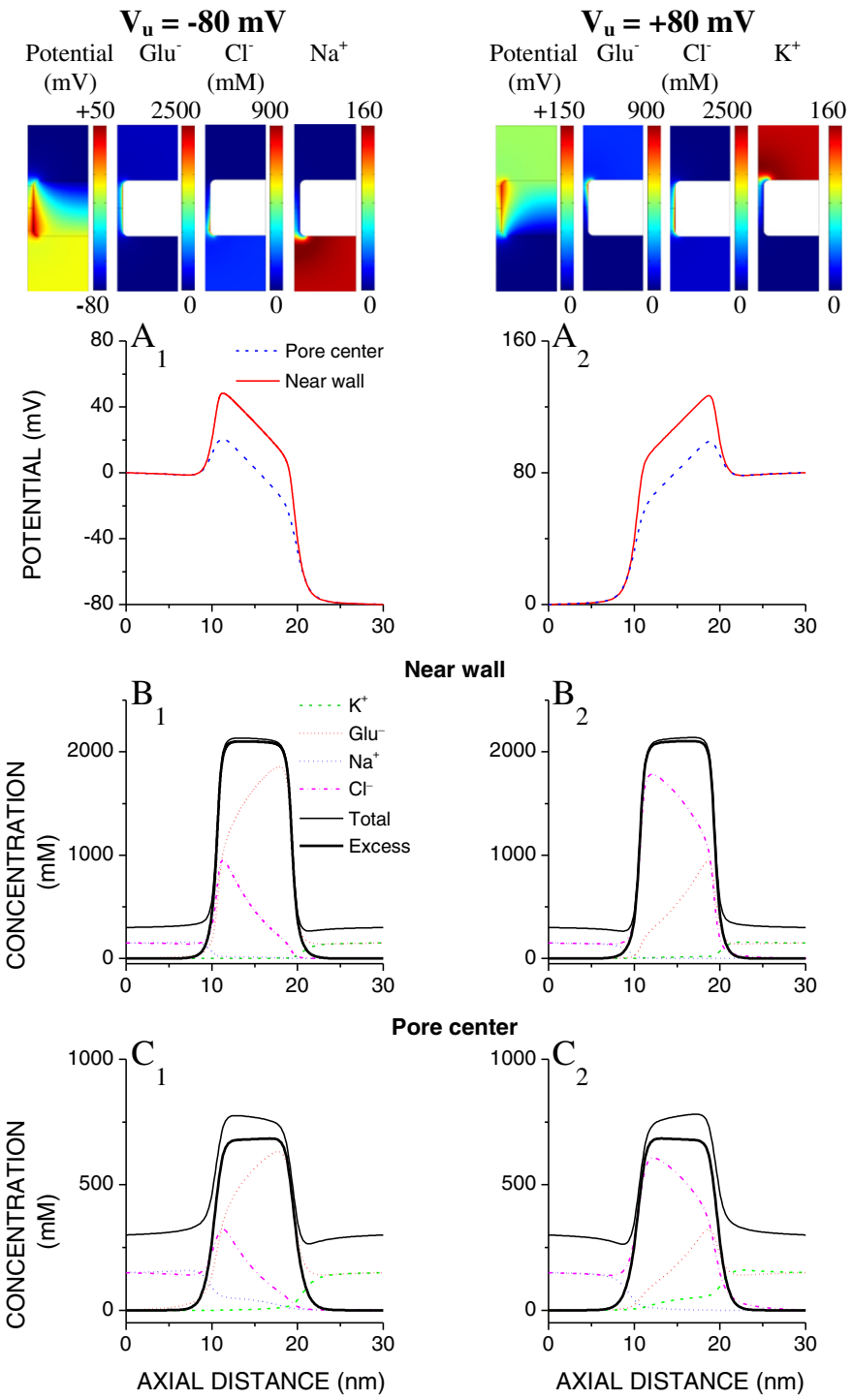

Fig. 2. The effect of the voltage bias on the potential and ion concentration spatial profiles in a uniformly and positively charged nanopore. The color coded 2D distributions of the potential and of counter-ion (Glu^- and Cl^-) concentrations as wall as those of co-ions (Na^+; left panel or K^+; right panel) are shown on the top for a narrow (r = 1 nm) nanopore. Calibration bars are as indicated. A_1–A_2) Potential profiles. B_1–B_2) The ion concentration profiles, their sum (total) and the excess (cation minus anion) concentration near the wall. The co-ions are excluded, whereas the counter-ion concentrations are high. Glu^- predominates throughout the nanopore if V_u is negative (regular bias), and Cl^- if it is positive (reverse bias). C_1–C_2) In the pore center the concentration profiles are qualitatively similar, but lower and the exclusion of the co-ions is less pronounced. The potential at the upper controlling edges (V_u) was −80 mV (left panels) or +80 mV (right panels), but at the lower controlling edges V_d was in both cases 0 mV. The pressure at the upper (p_u) and lower (p_d) controlling edges was 500 kPa and 0 Pa, respectively. K^+–glutamate$^-$ was 150 mM and Na^+–Cl^- 0 mM (upper edges), and reverse at the lower edges. Charge density on the pore wall was +64 mC/m^2.

in a uniformly and positively charged nanopore. They are shown to assess the changes induced by the pore wall charge patterning in unipolar and bipolar nanopores (see below). When nanopore is narrow (r = 1 nm), the fluxes are largely carried by counter-ions (Glu^- and Cl^-), and are higher near the charged wall surface (Fig. 6B and E), whereas those of co-ions (K^+ and Na^+) are much lower, and largely confined to the pore center (Fig. 6C and F). The voltage bias strongly influences all fluxes. With regular bias Glu^- downward flux clearly predominates over Cl^- upward flux (Fig. 6A–B), whereas the much smaller upward Na^+ flux is greater than the downward K^+ flux (Na^+ and K^+ are co-ions; Fig. 6C). If the bias is reverse the inward Cl^- flux predominates, the outward Glu^- flux is negligible (Fig. 6D–E), but downward K^+

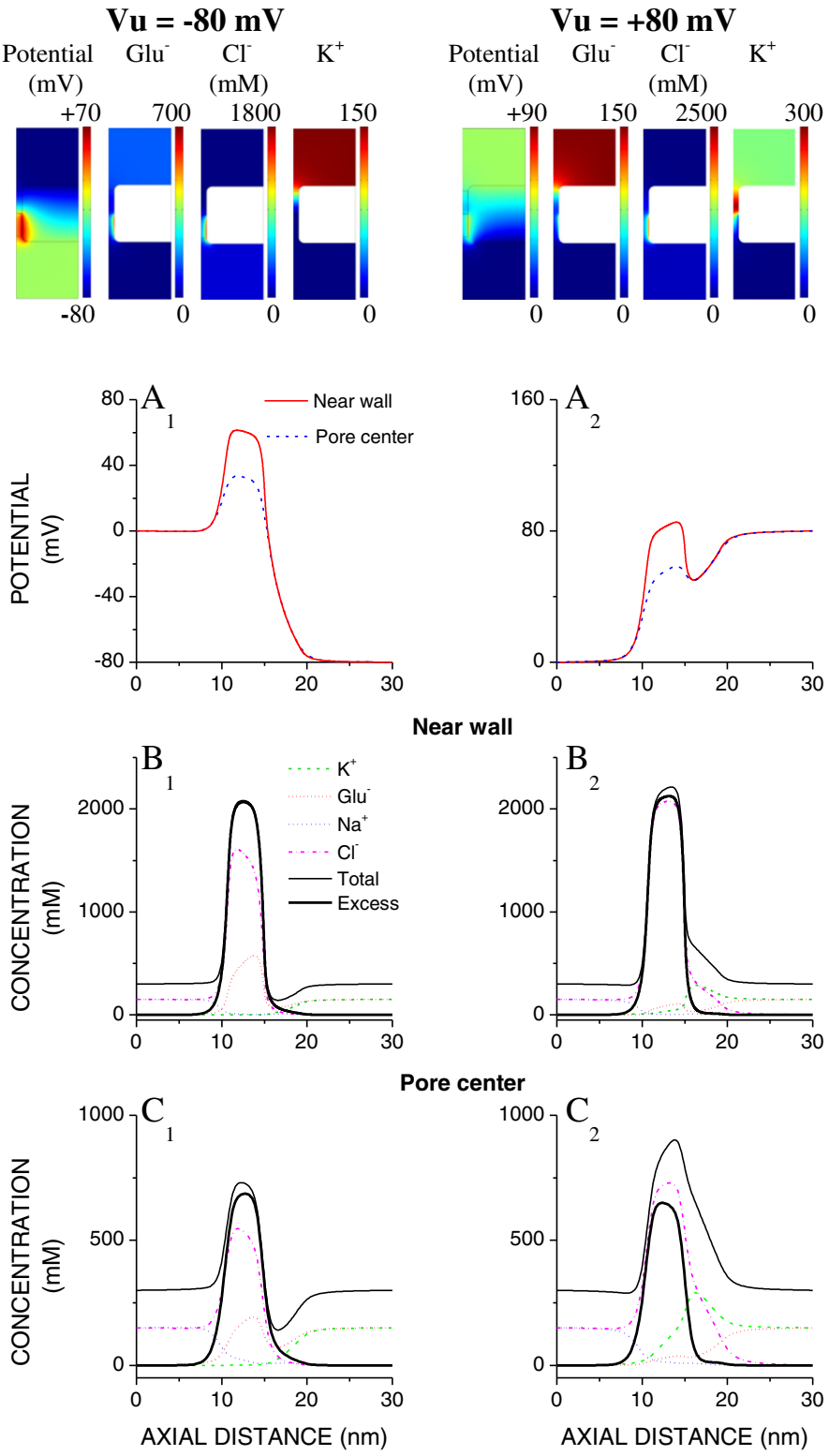

Fig. 3. The effect of voltage bias on the potential and ion concentration spatial profiles in uni-polar and positively charged nanopores (lower half charged). The color coded 2D distributions of the potential and of counter-ion (Glu^- and Cl^-) concentrations as wall as Na^+ (co-ion) are shown on the top for a narrow (r = 1 nm) nanopore. Calibration bars are as indicated. A_1–A_2) Potential profiles (near the wall and in the pore center) are very different depending on the voltage bias. B_1–B_2) Concentration profiles of individual ions, of their sum (total) and of ion excess near the wall. In the charged (lower) half of the nanopore the concentration of counter-ions is very high regardless of voltage bias. If the bias is regular Cl^- predominates, but if it is reverse Glu^- and Cl^- are both present, though Cl^- predominates. In uncharged half and with regular bias the Cl^- concentration remains high and K^+ is present, but if the bias is reverse all ion concentrations are low. The excess concentration, which is high and almost constant in the charged half rapidly becomes zero in the uncharged half. C_1–C_2) In the pore center the ion concentration profiles are similar to those near the wall, but lower and the exclusion of the co-ions is less pronounced. V_d was in both cases 0 mV. The p_u was 500 kPa and p_d was 0 kPa. Charge density on the upper half of the pore wall was +64 mC/m^2.

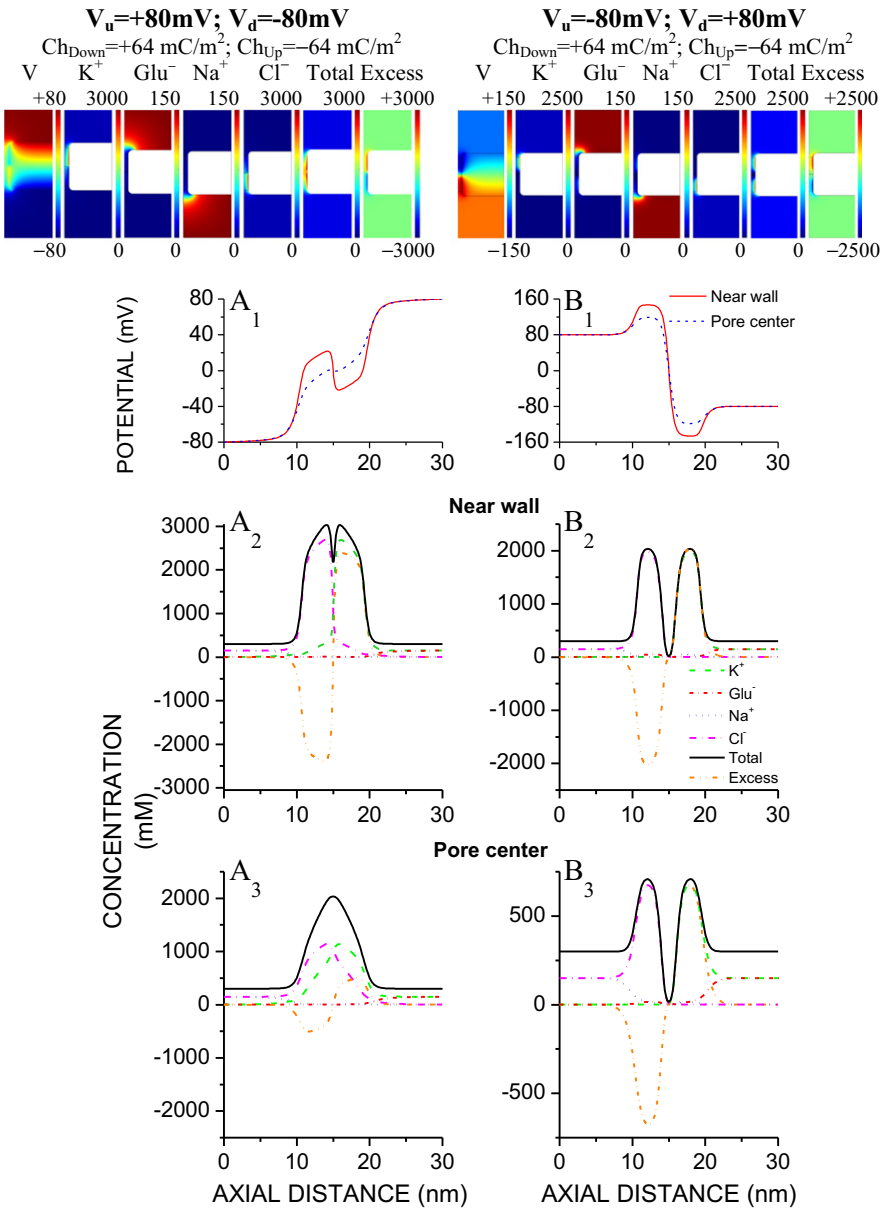

Fig. 4. In bi-polar nanopores the voltage bias influences greatly the profiles of the potential and of the ion concentrations, even near the wall. The color coded 2D distributions of the potential, the ion concentrations (K^+, Glu^-, Na^+ and Cl^-), their sum (total) as wall as the excess concentration (cation minus anion concentration) are shown on the top for a narrow (r = 1 nm) nanopore. Left panels — regular bias; right panels — reverse bias. Calibration bars are as indicated with voltages given in mV and concentrations in mM. A_1–B_1) Potential profiles near the wall and in the pore center. A_2–B_2) Ion concentration profiles near the wall. In each pore half the counter-ion from the adjacent compartment dominates regardless of bias, but the co-ions may also be present with regular bias, but are almost completely absent with reverse bias. The total concentration (sum of all ion concentrations) dips midway (axially) with regular bias, but no ions of any kind are present if the bias is reverse near the wall (B_2) or in the pore center (B_3). A_3–B_3) Ion concentration profiles in the pore center. In each pore half the counter-ion from the adjacent compartment dominates regardless of bias. If the bias is regular the contribution of co-ions (that are counter-ions in the other half) is very significant and midway (axially) the total concentration peaks (A_3), but if the bias is reverse there are essentially no ions of any kind midway (B_3). V_u, V_d and the charge density on the lower and upper half of the pore wall were as indicated. On the upper controlling edges the concentrations of K^+–glutamate$^-$ and Na^+–Cl^- were 150 mM and 0 mM respectively, whereas on the lower controlling edges they were 0 mM and 150 mM. The p_u was 500 kPa and p_d was 0 Pa.

flux, though very small is greater than the upward Na^+ flux (Fig. 6F). Finally, note that the radial profiles of all ion fluxes at the upper and lower virtual edges are very similar, and that the higher the ion concentration within the nanopore the higher its flux.

The secretory vesicles contain Ca^{2+} [28], and we now assess how this may affect the flux of other ions or charged particles. Fig. 7 gives the 2D color plots of the axial fluxes in a uniformly and negatively charged narrow (r = 1 nm; the charge density was −64 mC/m^2) nanopore, in the absence (upper panels) and in the presence of 10 mM Ca^{2+} in the intra-vesicular compartment (lower panels). V_u was either −80 mV (left panels) or +80 mV (right panels). We only show the fluxes in the negatively charged nanopore, because Ca^{2+} (as a co-ion) does not enter into the positively charged nanopore (even when comparatively wide; not shown) and its effect on the axial fluxes of other ions is minimal. As both the plots of the axial (Fig. 7A_1–A_2 and C_1–C_2) and radial fluxes reveal (Fig. 7B_1–B_2 and D_1–D_2), the fluxes are almost entirely carried by counter-ions. If V_u = −80 mV the Na^+ flux dominates, and Ca^{2+} presence in the upper (intra-vesicular compartment) does not visibly

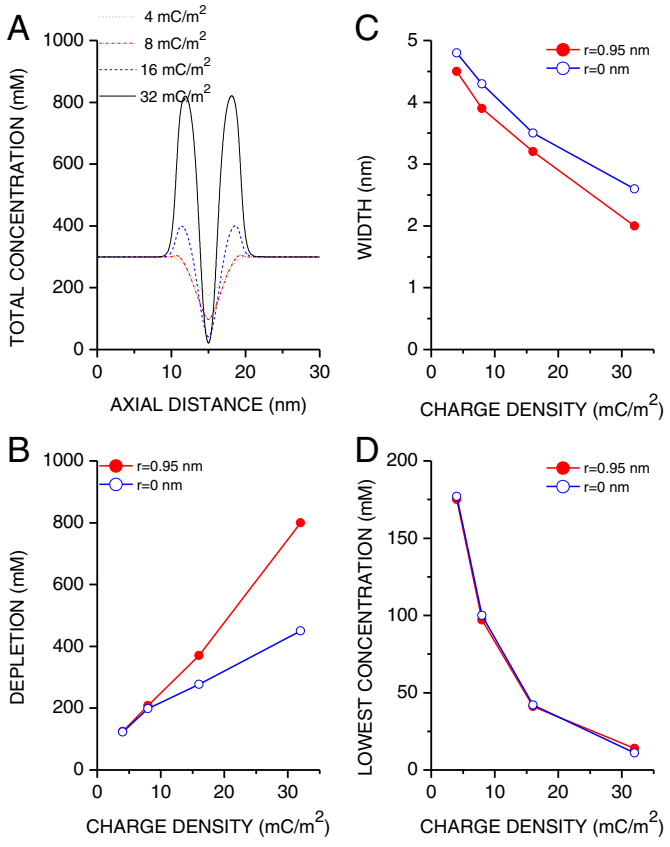

Fig. 5. In bi-polar nanopores under reverse voltage bias, depletion of the total ion concentration in the middle of the nanopore becomes greater, but narrower at higher fixed charge density. A) The axial profiles of the total ion concentration near the wall ($r = 0.95$ nm) for four different charge densities as indicated. B) The total ion concentration depletion (defined as the difference in concentration between maximal and minimal value) rises as the charge density increases, but more near the wall than in the pore center ($r = 0$ nm). C) The width at 50% depletion diminishes as the charge density rises. D) The total concentration diminishes to a lower level at higher charge densities. V_u and V_d were −80 mV and +80 mV respectively. On the upper controlling edges the concentrations of K^+–glutamate$^-$ and Na^+–Cl^- were 150 mM and 0 mM respectively, whereas on the lower controlling edges they were 0 mM and 150 mM. The p_u was 500 kPa and p_d was 0 Pa.

alter it or other fluxes, but if $V_u = +80$ mV the K^+ flux, which now dominates, is reduced if Ca^{2+} is present in the upper (intra-vesicular compartment), being replaced by the Ca^{2+} flux.

3.5. Ion fluxes in unipolar nanopores

Charge patterning on the wall of the unipolar nanopores leads to profiles of axial and radial ion fluxes that are very different from those of the uniformly charged pores. Axial ion fluxes near the wall are fairly constant axially within each half (charged or uncharged), are higher near the charged half than near the uncharged half, and change rapidly in the middle of the nanopore where the charged and uncharged halves meet (Fig. 8A and D). Unlike the case in the uniformly charged pores the dominant counter-ion flux always comes from the compartment flanking the charged half of the nanopore regardless of the voltage bias. With charging pattern as shown the Glu^- flux dominates if V_u is negative (reverse bias). The Cl^- flux is not dominant, but its flow deserves a comment. In the lower (charged) half Cl^-, ions move upwards near the wall, but in the pore center they move downwards (Fig. 8B; see also fourth left panel). Near the wall, Cl^- ions are attracted by the positive charges on the wall, whereas in the pore center they are repelled by the potential gradient along the axis of the nanopore. If V_u is positive (regular bias) the Cl^- flux dominates. In the pore center of the uncharged half the Cl^- flux is greater than in the center of the charged half (no ion sinks or sources in the pore), and its radial distribution becomes quite uniform radially. Finally, note that both counter-ion fluxes (Glu^- and Cl^-) near the wall of the charged half are clearly lower than those near the wall of the uniformly charged nanopore with the same charge density (Fig. 6A and D). The co-ion fluxes are smaller. Na^+ and K^+ fluxes dominate for reverse and regular bias respectively, but the K^+ flux is clearly greater (Fig. 8C and F).

3.6. Diffusive, migratory and convective fluxes in uniformly charged and in unipolar nanopores

To further elucidate the nature of the ion flow within the nanopore we evaluated what contribution the convective, diffusive and migratory fluxes make to the overall ion flux. We restrict our attention to Glu^- and Cl^- fluxes, as these are counter-ions and dominate the ion flow through positively charged nanopores (uniformly charged or unipolar). Given that the nanopores evaluated in this study are very narrow ($r = 1$ nm), it is to be expected that the convective flux of any ion will be very small, and this is the case (Fig. 9). As shown above (Figs. 2 and 3) the concentration and the potential gradients in the unipolar (but also in the uniformly charged) nanopores are very high near points where charged and uncharged parts are in contact. The diffusive and migratory axial ion fluxes ought also to be high near such points, and they are. As Fig. 9A–C show they are indeed both very prominent where the charged part of nanopore meets the uncharged part, but they oppose each other though not completely. We also show the Cl^- diffusive and migratory fluxes with lower half charged. They are larger (their diffusion constant is greater than that of Glu^-), but they oppose each other more completely, and as a result their sum is even smaller, though not negligible (Fig. 9D).

3.7. Ion fluxes in bipolar nanopores with regular and reverse bias

The ion fluxes in the bipolar nanopores are the result of same influences — the voltage bias and the potential generated by the fixed charges on the pore wall, and concentration gradients. However, the charge distribution is different, and the fluxes more complex. Both bipolar nanopores we evaluated had the upper half negatively charged and the bottom half positively charged, and the charge density was in both cases the same (64 mC/m^2). The bias was changed by altering the V_u and V_d ('Regular bias'; $V_u = +80$ mV and $V_d = -80$ mV or 'Reverse bias' — $V_u = -80$ mV and $V_d = +80$ mV).

If the bias is reverse, all ion fluxes are very small, but deserve detailed description (Fig. 10). K^+ ions are counter-ions in the upper half, and the concentration gradient tends to move them downwards, the external electric field tends to move them upwards, and the electrical field due to the fixed (negative) charges tends to move them towards the wall. As a result of these forces in the upper half in the pore center they move downwards, but near the wall they move upwards (Fig. 10A_1–C_1). They do not enter in the lower half (Fig. 10D_1 and D_{2a}). The radial K^+ ion fluxes in the upper half of the nanopore are negative (i.e., towards the center; Fig. 10C_{2a}), and zero in the lower half (Fig. 10A_2). Cl^- ions (they are co-ions in the negatively charged upper half and counter-ions in the positively charged lower half) are influenced by similar forces. Their axial flux is zero in the upper half (Fig. 10A_1–C_1). In the lower half it is upwards near the wall (Fig. 10A_1 and D_1), but downwards in the pore center (Fig. 10B_1 and D_1). Cl^- ions also remain in the same half of the nanopore where they entered. Thus both ions that entered the corresponding half of the nanopore as counter-ions do not go through the nanopore.

Glu^- and Na^+ enter as co-ions at opposite ends of the nanopore. Glu^- ions move downwards in the upper half, and being co-ions their flux is very small and present largely in the pore center. In the lower part, where they are counter-ions, they continue moving downwards,

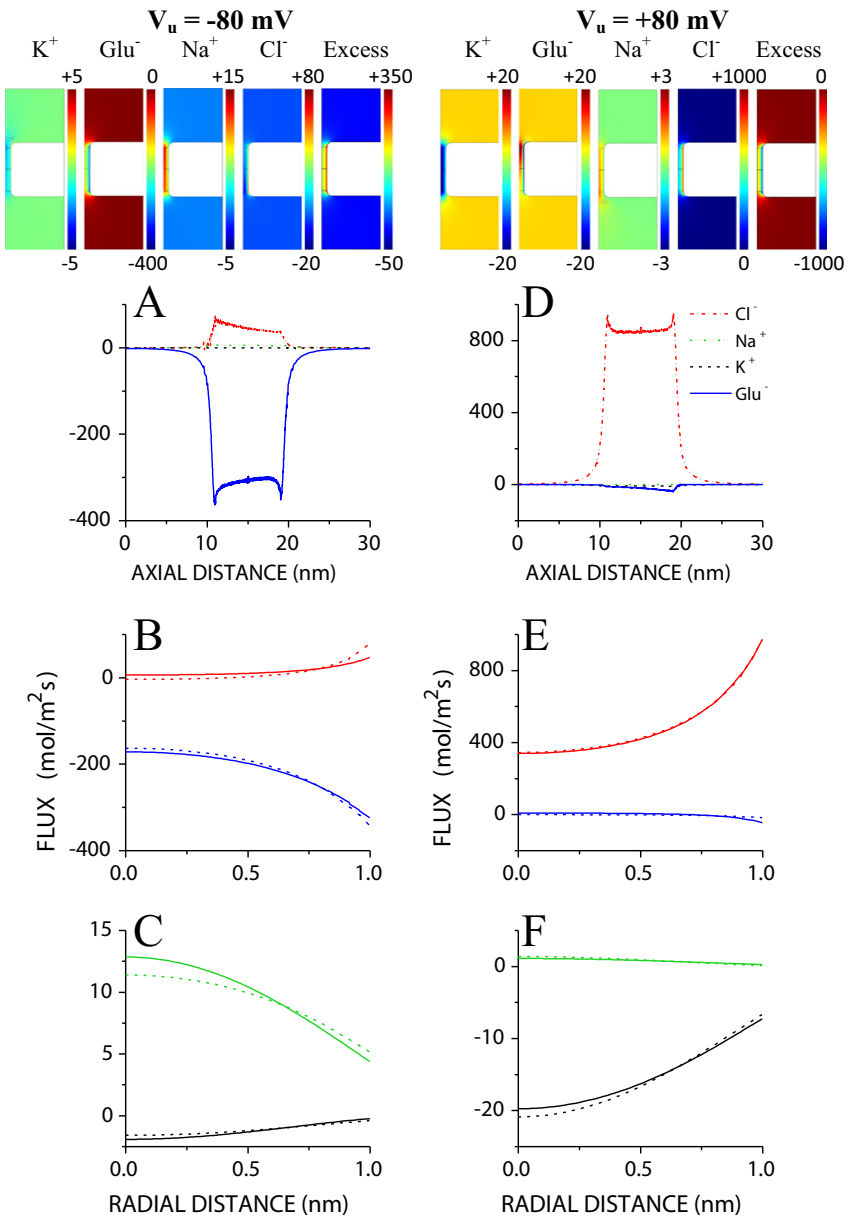

Fig. 6. Which counter-ion dominates the flux in a narrow uniformly charged nanopore is determined by the voltage bias. The color coded 2D distributions of the ion fluxes in the axial direction are shown. Calibration bars are as indicated; the fluxes are in mol/(m^2s). A and D) Axial profiles of the axial ion fluxes near the wall. If V_u is −80 mV Glu^- flux (outward) predominates, but Cl^- flux (inward) is not negligible (A). If V_u is +80 mV the inward ion flux is almost entirely Cl^-. B–C and E–F) Radial profiles of the axial ion fluxes (solid lines — ion fluxes at the upper virtual edge; dashed lines — ion fluxes at the lower virtual edge). The profiles of all ion fluxes at the upper and lower virtual edges are very similar. Near the wall the fluxes of counter-ions rise (in absolute value), and those of co-ions diminish. The charge density on the pore wall was +64 mC/m^2. V_d is 0 mV in all cases. On the upper controlling edges the concentrations of K^+–glutamate$^-$ and Na^+–Cl^- were 150 mM and 0 mM respectively, and on the lower controlling edges they were 0 mM and 150 mM. The p_u was 500 kPa and p_d was 0 Pa.

but near the wall (Fig. 10A_1–D_1). Note that the radial Glu^- flux is positive in the middle of the nanopore, indicating the movement of Glu^- ions towards the wall (Fig. 10B_2). The radial Glu^- fluxes are also pronounced near the wall at the entry (i.e. at the upper end) and at the exit (i.e. at the lower end). The Na^+ ion flux can be considered as a mirror image of the Glu^- flux. Na^+ ions enter from the lower compartment into the nanopore as co-ions and move upwards largely in the pore center. In the upper half they continue upwards, but near the wall (Fig. 10A_1–D_1). Finally, the excess flux (defined as the difference of the cation and anion fluxes) is upwards, but in the upper half it is near the wall and in the lower half in the center (Fig. 10A–B). With reverse bias the current through the pore is very small being carried not by counter-ions but by co-ions.

The ion fluxes are much greater if the bias is regular, and have different axial and radial profiles. The excess flux is entirely dominated by the flux of ions entering the pore as counter-ions (Fig. 11A_1–D_1). K^+ (a counter-ion in the upper half) flows downwards largely near the wall, and continues downwards, but in the pore center (Fig. 11A_1). As expected its radial flux is negative in the middle of the nanopore (Fig. 11A_2). The Cl^- (counter-ion in the lower half of the nanopore) flux mirrors that of the K^+ flux. Cl^- moves upwards near the positively charged wall, and continues upwards in the upper half of the nanopore (where it is a co-ion), but near the pore center (Fig. 11A_1–D_1). Glu^- and Na^+ fluxes (Glu^- is a co-ion in the upper half and Na^+ in the lower half of the nanopore; i.e., at their corresponding entry points) are much smaller and can be ignored. Finally, note that the excess flux, which is quite

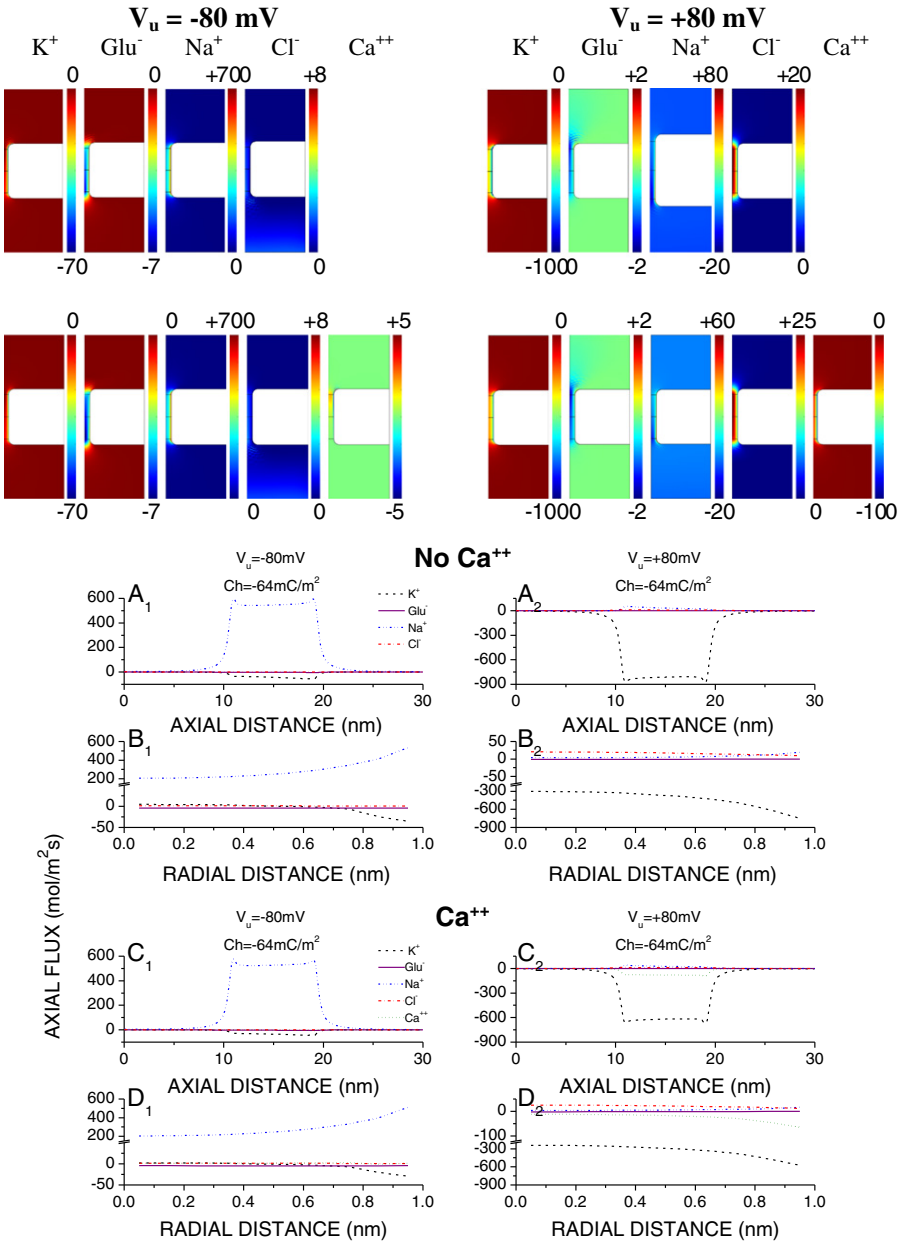

Fig. 7. Intravesicular Ca^{2+} reduces the flux of other cations from the vesicle, but the effect is limited. The 2D color coded distributions of the axial ion fluxes are shown. Calibration bars are as indicated; the fluxes are in mol/(m^2s). The axial profiles of the axial ion fluxes near the wall in the absence of Ca^{2+} in the upper compartment (A_1; $V_u = -80$ mV; A_2; $V_u = +80$ mV), and in the presence of 10 mM Ca^{2+} (C_1; $V_u = -80$ mV; C_2; $V_u = +80$ mV). The radial profiles of the axial ion fluxes near the wall in the absence of Ca^{2+} in the upper compartment (B_1; $V_u = -80$ mV; B_2; $V_u = +80$ mV), and in the presence of 10 mM Ca^{2+} (D_1; $V_u = -80$ mV; D_2; $V_u = +80$ mV). If V_u is −80 mV the inward Na^+ flux (moving upwards) clearly predominates, and Ca^{2+} presence in the upper compartment does not alter it. However, if V_u is +80 mV the outward K^+ flux (moving downwards) is reduced if Ca^{2+} is present in the upper compartment. The V_d is 0 mV in all cases. In the absence of Ca^{2+} on the upper controlling edges the concentrations of K^+–glutamate$^-$ and Na^+–Cl^- were 150 mM and 0 mM respectively, and on the lower controlling edges they were 0 mM and 150 mM. If Ca^{2+} (10 mM) was present in the upper compartment, the K^+ concentration on the upper controlling edges was reduced to 130 mM. The p_u was 500 kPa and p_d was 0 Pa.

uniform radially and axially, is negative (Fig. 11A_1–D_1; see also the color 2D panels).

4. Discussion

4.1. Background information

In free solution, conductivity is largely determined by the ion concentration, increasing as the ion concentration rises. However, in nanopores the ions come into close contact with the pore wall and its charges. Pore conductivity is therefore significantly influenced by the pore radius, fixed charge density and charge patterning on the pore wall, as well as voltage bias and the concentration of ions outside of nanopore [19]. Moreover, the conductivity is spatially non-uniform within unipolar and especially bipolar nanopores. To better understand what determines the conductivity within nanopores we evaluated how the potential, the ion concentrations and finally the fluxes are distributed within such nanopores, and how these distributions are influenced by the voltage bias and the fixed charges on the pore wall. We focused on short (10.0 nm long) cylindrical and generally narrow (1–4 nm radius) nanopores. They are of great interest in biology, because fusion pores and to a lesser extent, ion channels have similar geometry, but

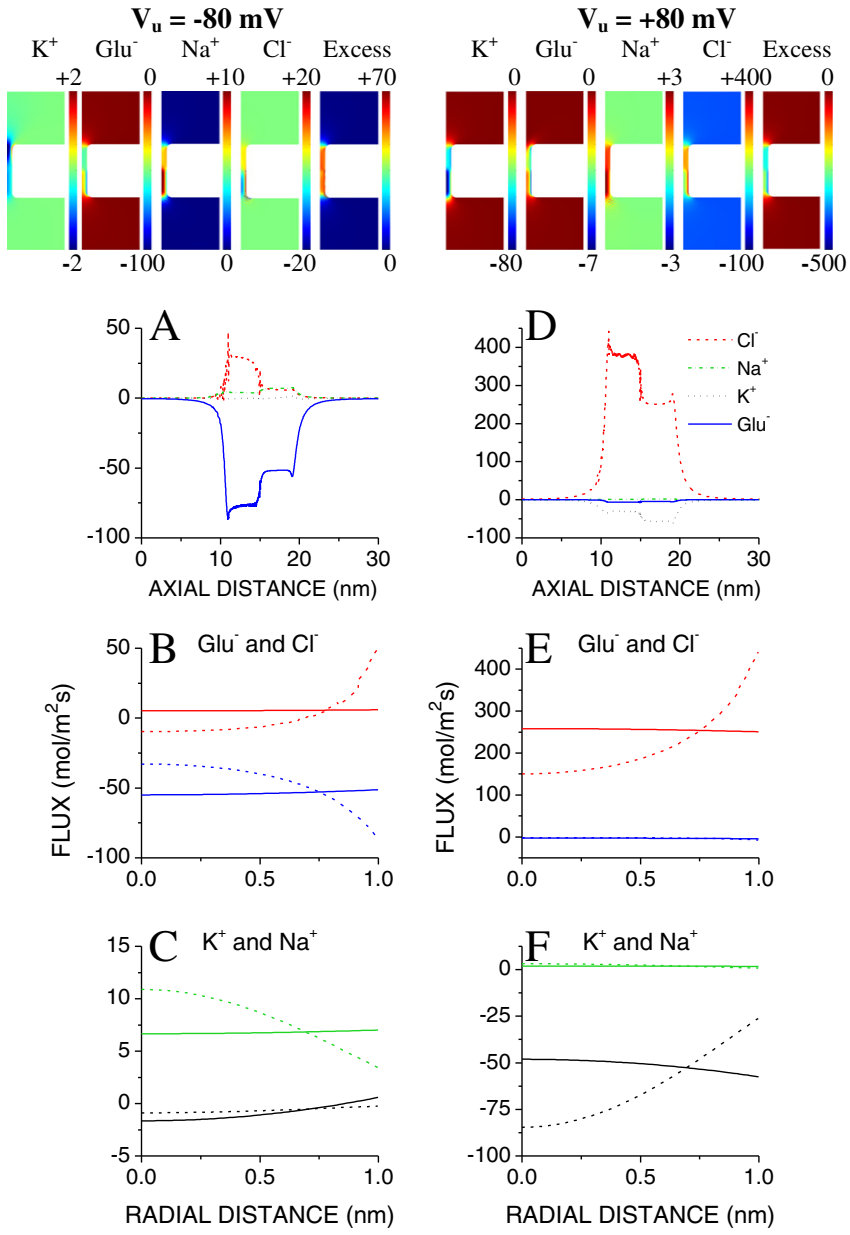

Fig. 8. The counter-ion dominating the ion flux in unipolar nanopores comes from the compartment flanking the charged half of the pore. The color coded 2D distributions of axial ion fluxes are shown on the top (left panels — reverse bias; $V_u = -80$ mV; right panels — regular bias; $V_u = +80$ mV). $V_d = 0$ mV in both cases. Calibration bars are as indicated; the fluxes are in mol/(m^2s). A and D) The axial profiles of axial ion fluxes near the wall with reverse bias (A) and with regular bias (D). If the V_u is negative (reverse bias; A) the Glu^- flux is negative (i.e., downwards) and significant, but if it is positive (regular bias; D) it is near zero. In contrast the Cl^- flux is much smaller and positive (i.e., upwards) near the wall in the lower (charged) half if the bias is reverse (A), becoming very pronounced if the bias is regular (D). B, E, C and F) The radial profiles of axial ion fluxes (solid line — ion fluxes at the upper virtual edge; dashed line — ion fluxes at the lower virtual edge). B and E) Regardless of voltage bias, as expected, the radial profiles of counter-ions (Glu^- and Cl^-) fluxes are higher near the pore wall in the lower (charged) half, but are uniform in the upper (uncharged) half. Interestingly the Cl^- flux is positive (upwards) near the wall, but is downwards (negative) in the pore center in the lower (charged) half of the nanopore (B) if the bias is reverse. C and F) The radial profiles of co-ion (K^+ and Na^+) fluxes (also uniform in the upper — uncharged half), are lower near the wall in the lower (charged) half regardless of bias. If the V_u is negative (reverse bias) the K^+ flux is near zero throughout the nanopore, whereas the Na^+ flux is positive. If the V_u is positive (regular bias) the Na^+ flux is nearly zero throughout the pore, whereas the K^+ flux is negative. The charge density on the wall of the lower half of the nanopore was +64 mC/m^2. On the upper controlling edges the concentrations of K^+–glutamate$^-$ and Na^+–Cl^- were 150 mM and 0 mM respectively, whereas on the lower controlling edges they were 0 mM and 150 mM. The p_u was 500 kPa and p_d was 0 Pa.

also in engineering as the miniaturization of nanofluidic devices progresses. We considered three idealized situations — uniformly charged, unipolar (one half charged and another half uncharged) and bipolar (both halves charged with the same charge density, but with opposite polarity) nanopores, and explore the differences induced by the voltage bias (regular and reverse).

The problem was approached numerically. Whereas analytical solutions are available for slit pores [29,30], there is no analytical solution to the Poisson–Nernst–Planck equations for cylindrical pores [30]. An additional limitation is that we study very short (10.0 nm length) nanopores, whereas the analytical solutions are better suited for the analysis of very long nanopores. Our simulations included external reservoirs, and this is relevant because the nanopores are very short, and conductivity changes significantly not only inside the pore but also in the regions near the pore entrance [19]. We thus needed to evaluate how ionic concentration and electric potential change outside of the nanopore.

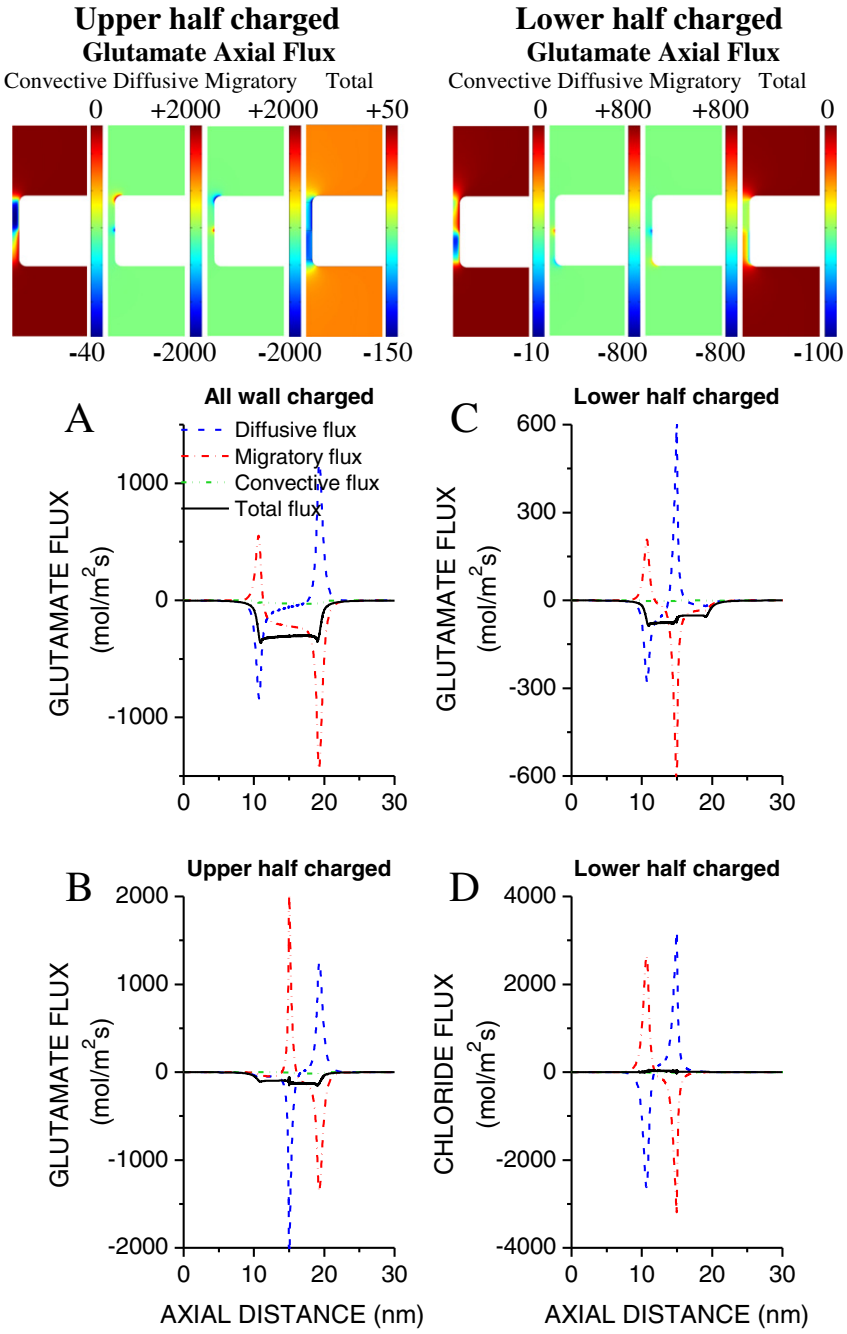

Fig. 9. The diffusive and migratory fluxes of counter-ions are very large near the points where the charged and un-charged parts of the pore wall meet, but oppose each other. The color coded 2D distributions of the axial Glu^- fluxes of two uni-polar nanopores, one with charged upper half (left panels; regular bias), and another with charged lower half (right panels; reverse bias) are shown. Calibration bars are as indicated, and the fluxes are in mol/(m^2s). A) In a uniformly charged nanopore the axial diffusive and migratory Glu^- fluxes near the wall are very pronounced at both ends, but oppose each other. The total axial Glu^- flux within the nanopore (including at both ends) is small, negative and fairly constant. B–C) In a uni-polar nanopore (with the upper half charged; B or the lower half; C) the diffusive and migratory Glu^- fluxes in the middle of the nanopore are very large. The total flux is fairly constant in both halves, but higher in the charged half. D) Diffusive and migratory Cl^- fluxes are even greater in a unipolar nanopore (lower half charged). The total flux is negligible as they almost completely balance each other. Regardless of whether the nanopore is uniformly charged or is unipolar the convective fluxes are very small. The charge density on the charged parts of the wall of the uniformly charged and unipolar nanopores was +64 mC/m^2. V_u was−80 mV and V_d was 0 mV. On the upper controlling edges the concentrations of K^+–glutamate$^-$ and Na^+–Cl^- were 150 mM and 0 mM respectively, whereas on the lower controlling edges they were 0 mM and 150 mM. The p_u was 500 kPa and p_d was 0 Pa.

4.2. Potential and concentration profiles in uniformly charged, unipolar and bipolar nanopores

The axial potential profiles in uniformly charged nanopores are 'simple' — ascending or descending depending on the voltage bias, but the charge patterning on the wall makes them more complex by enhancing or depressing them or both. The changes are spatially highly localized, as are those of ion concentrations. As indicated by the excess concentration (the concentration difference between counter-ions and co-ions) the approximate charge neutrality is maintained down to a very small scale. In a narrow (r = 1 nm) unipolar nanopore the excess concentration diminishes from >600 mM in the charged half of the pore to essentially zero in the uncharged half over a distance of 1–2 nm near the wall. Even in the pore center the change is very rapid. In bipolar nanopores

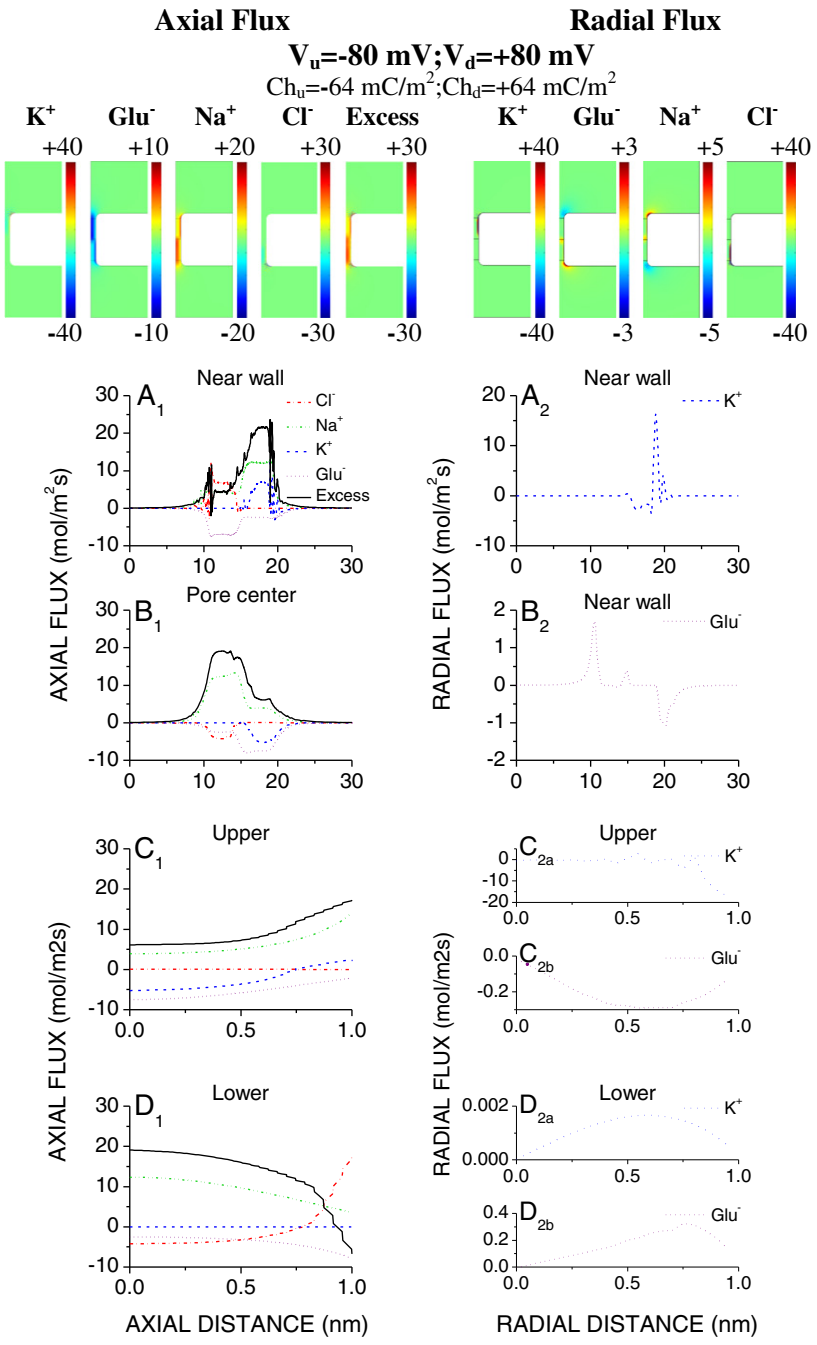

Fig. 10. Axial and radial ion fluxes in a bi-polar nanopore with reverse bias. The color coded 2D distributions of the axial fluxes of the individual ions and of the excess flux defined as the difference between cation and anion fluxes (left panels), and of the radial fluxes (right panels). Calibration bars are as indicated; the fluxes are in mol/(m^2s). A_1–B_1) The axial profiles of axial ion fluxes and of the excess flux near the wall (A_1), and in the pore center (B_1). C_1–D_1) The radial profiles of the axial ion fluxes and of the excess flux at the upper (C_1) and lower (D_1) virtual edges. A_2–B_2) The axial profiles of the radial K^+ (A_2) and Glu^- (B_2) fluxes. C_2–D_2) The radial profiles of the radial K^+ and Glu^- fluxes at the upper (C_{2a}–C_{2b}) and lower (D_{2a}–D_{2b}) virtual edges. Note how small the fluxes (axial and radial) of counter-ions are, much smaller than in the bipolar nanopore with a regular bias, and are comparable in amplitude to those of co-ions. The V_u and V_d, and the charge density on the walls (upper and lower half) of the nanopore are as indicated. On the upper controlling edges the concentrations of K^+–glutamate$^-$ and Na^+–Cl^- were 150 mM and 0 mM respectively, whereas on the lower controlling edges they were 0 mM and 150 mM. The p_u was 500 kPa and p_d was 0 Pa.

the excess concentration (estimated as the concentration difference between cations and anions) changes similarly rapidly in the middle where two halves with charges of the opposite polarity meet. Note that its values are almost identical in charged parts of the unipolar, bipolar or uniformly charged nanopores, if the charged parts have the same charge density and the spatial distribution is very little influenced by the voltage bias. In uncharged parts it is very near zero. The voltage bias largely determines what counter-ion dominates in uniformly charged nanopores, but in unipolar nanopores the counter-ion from the compartment near the charged half dominates, whereas in bipolar nanopores the counter-ion with the highest concentration in each half is from the adjacent compartment.

Interest in individual nanopore ionic devices, such as ionic diodes that rectify the ionic current, and ionic filters that can control what ions are transported through the nanopore is growing [8,10,12,13,31]. Engineered nanopores often rectify. Even when the surface charges on the wall are homogeneous the rectification is observed if they are conically shaped [9,32]. Whether the resistance of long bipolar nanopores is

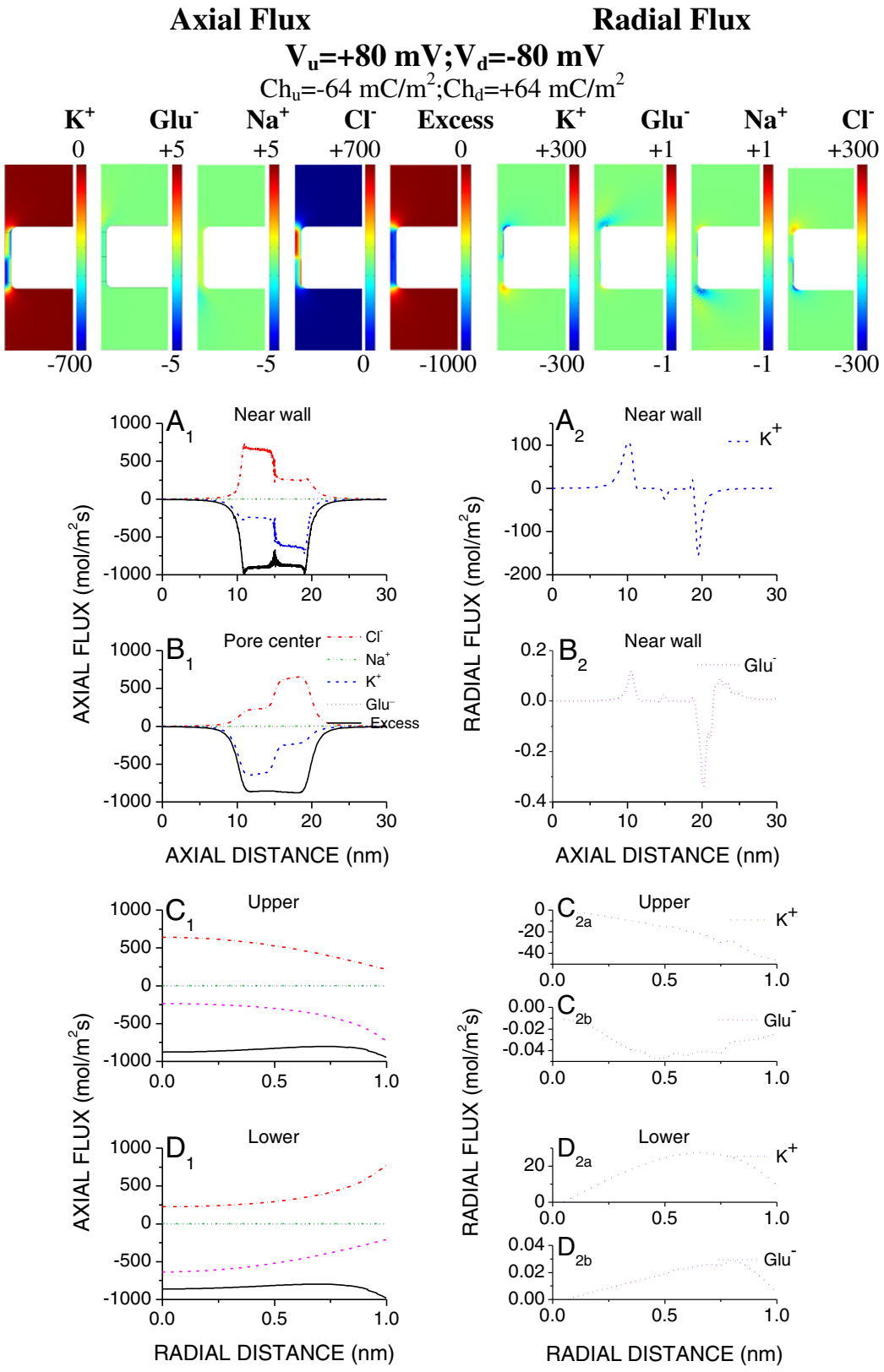

Fig. 11. Axial and radial ion fluxes in a bipolar nanopore with regular bias. The color coded 2D distributions of the axial fluxes of the individual ions and of the excess flux defined as the difference between cation and anion fluxes (left panels), and of the radial fluxes (right panels) are shown. Calibration bars are as indicated; the fluxes are in mol/(m2s). A_1–B_1) The axial profiles of axial ion fluxes and of the excess flux near the wall (A_1), and in the pore center (B_1). C_1–D_1) The radial profiles of the axial ion fluxes and of the excess axial flux at the upper (C_1) and lower (D_1) virtual edges. A_2–B_2) The axial profiles of the radial K+ (A_2) and Glu− (B_2) fluxes. C_1–D_1) The radial profiles of the radial K+ and Glu− fluxes at the upper (C_{2a}–C_{2b}) and lower (D_{2a}–D_{2b}) virtual edges. Two fluxes that start as counter-ion fluxes are dominant (K+ in the upper half and Cl− in the lower half). K+ starts moving downward largely near the negatively charged wall of the upper half of the nanopore, but in the middle of the nanopore it moves radially towards the center, and continues moving downward but largely in the pore center. The movement of Cl− is similar, but in the opposite direction. The axial excess flux is quite uniform both axially and radially. The current that traverses the pore is thus largely carried by counter-ions and it is quite large. The V_u and V_d, and the pore wall charge density are as indicated. On the upper controlling edges the concentrations of K+–glutamate− and Na+–Cl− were 150 mM and 0 mM respectively, whereas on the lower controlling edges they were 0 mM and 150 mM. At the upper controlling edges the pressure was 500 kPa and at the lower edges 0 Pa.

low or high is explained by the level of ion depletion/accumulation in the middle of the pore (as both cations and anions move to the outside) and is produced by the voltage bias. If the bias is regular both cations and anions accumulate in the middle leading to large ionic current and low resistance, and if it is reverse it leads to depletion [10,33]. This should lead to very high resistivity in the middle of short cylindrical bipolar nanopores under reverse bias, especially near the wall; i.e. in the areas of high ion depletion. The extent of depletion of the total ion concentration is greater and the minimum reached is lower at higher charge densities. However, the width of the depletion layer is narrower. Even with regular bias (i.e., where the concentration and conductivity are high within the nanopore) the total ion concentration dips near the wall in the middle. However, if the bias is reverse the conductivity will be much reduced not only in the areas of high ion depletion, but probably throughout the nanopore [19].

4.3. Ion fluxes in uniformly charged and unipolar nanopores

To gain greater insight into what factors determine the pore's rectification and its resistivity in general we explore its ionic basis, i.e., what ion fluxes dominate, what their spatial distributions are, and what changes are induced by the pore wall charge patterning and voltage bias. The ion fluxes we evaluated in the axial direction are termed axial fluxes. We first described fluxes in uniformly charged nanopores to evaluate changes induced by the wall charge patterning. As expected in uniformly charged nanopores axial fluxes change very little axially, but the counter-ion axial fluxes are greater near the wall (as are their concentrations). The opposite is true for co-ions and their axial fluxes. As expected the radial profiles of all axial ion fluxes at the upper and lower virtual edges were found to be very similar.

Secretory vesicles are known to contain significant amounts of Ca^{2+} [28]. Free intra-vesicular Ca^{2+} concentration changes during release of the vesicular content, as the vesicular interior comes into contact with the extracellular space. Although the resistance of the nanopore may not be affected if Ca^{2+} is present in the vesicle, this still may conceal the putative changes of the ionic and molecular fluxes (K^+, Na^+, Cl^- and Ca^{2+} and glutamate$^-$) through the nanopore. Such changes do occur, but depend on the voltage bias, which determines which counter-ion dominates the current through the nanopore. If the dominant flux is carried by K^+ ions, it will be reduced, albeit modestly, and will be 'replaced' by a smaller flux of a Ca^{2+} (divalent cation). If Na^+ flux dominates the intra-vesiclular Ca^{2+} presence has only a marginal effect.

In unipolar nanopores this simple rule (that the dominant counter-ion flux is carried by a counter-ion with the highest concentration) breaks down. Whereas the voltage bias determines which counter-ion flux dominates, this is not necessarily the counter-ion with the highest concentration within the charged half (which is the same as the counter-ion in the compartment flanking the charged half). With regular bias they are the same ion, and the ion flux is high, although not as high as in the uniformly charged nanopore. With reverse bias they differ, and the dominant counter-ion flux may be much smaller than with the regular bias. It is also much smaller than in the uniformly charged nanopore with the same external voltage and the same pore wall charge density.

The fluxes are also influenced by the diffusion constants. Two counter-ions in a positively charged nanopore are Cl^- and Glu^-, and the diffusion constant of Cl^- is 2.67 times higher than that of Glu^- (see Methods). If the lower half is charged (positively), the current within the nanopore is approximately five times greater with regular bias (Cl^- flux dominates) than with reverse bias (Glu^- flux dominates), but if the upper half is charged the current does not depend much on whether the bias is regular (Glu^- flux dominates) or reverse (Cl^- flux dominates). Regardless, the rectification ratio is in both cases low, as it should be given that the nanopore is very short [32].

Ionic selectivity was not the primary focus of this investigation. Nevertheless, we emphasize that, whereas the long unipolar nanopores are ion selective with current that is dominated by the counter-ion flux of the charged zone [33], in short nanopores other ions also contribute, though not greatly. For example if the lower half is charged and with a regular bias, the inward flux of Cl^- ions (counter-ions) is approximately five times greater than the outward flux of K^+ ions (co-ions). If the bias is reverse the outward flux of Glu^- ions is approximately four times greater than the combined inward flux of Cl^- ions and outward flux of Na^+ ions. An interesting finding is that in the charged half the Cl^- flux near the wall and in the pore center go in opposite direction, and the Cl^- flux only partly traverses the nanopore. Nevertheless, when lower or upper half is charged the ions in the uncharged half are similarly depleted if the bias is reverse. In conclusion, the rectification in unipolar nanopores results from the fact that with regular bias the counter-ion flux is carried by the counter-ions dominant in the charged half (which is thus greater), whereas in the reverse mode it is carried by the counter-ions not dominant in the charged half (which is thus smaller).

As expected the radial profiles of axial fluxes were found to be different in charged and uncharged halves of the unipolar nanopore, but it is surprising how quickly the change occurs. As can be seen from the axial fluxes they are fairly constant within each half of the nanopore (charged or uncharged), but at the junction of the two halves the amplitude of the flux changes completely over a distance of 1–2 nm. Near the wall of the uncharged half the counter-ion fluxes are lower (their radial profiles become more uniform), whereas in the charged half their radial profiles are quite non-uniform and higher near the wall.

Finally, we evaluated what contribution the convective, diffusive and migratory fluxes make to the overall ion flux. We restricted our attention to the counter-ion fluxes, as these are most often dominant. The convective fluxes were found to be very small as the nanopores are narrow. Given that the concentration and the potential gradients are high near the wall at the points where the charged and uncharged parts meet, the diffusive and migratory fluxes were also found to be high, but they oppose each other and the resulting flux was surprisingly small. Within charged or uncharged halves the diffusive and migratory fluxes were much smaller, but add to each other.

4.4. Ion fluxes in bipolar nanopores

Similar factors (the potential gradient generated by the voltage bias, the presence of fixed charges on the pore wall, the concentration gradient) influence the ion fluxes in bipolar nanopores. However, the charge distribution is more complex and this leads to some surprising outcomes. If the bias is reverse all ion fluxes are small, but deserve careful consideration. In a bipolar nanopore with a negatively charged upper half and positively charged lower half, the K^+ ion is a counter-ion in the upper half of the nanopore. How does it move? The concentration gradient would move it downwards, the voltage bias upwards and the fixed charges downwards and towards the wall. K^+ ions move downwards in the pore center and upwards near the wall, and do not enter into the lower half of the nanopore (the walls of the lower half are positively charged and the V_d is also positive). The flux of K^+ ions thus does not contribute to the pore conductance. The Cl^- flux largely resembles the K^+ flux. In the lower half (where Cl^- ions are counter-ions) Cl^- moves upwards near the wall, but does not enter into the upper half of the nanopore. Instead, Cl^- ions move towards the pore center, and in the pore center it moves downwards, and it thus also does not contribute to the pore conductance. The movements of the co-ions Glu^- and Na^+ are different. Glu^- moves downwards in the upper half, and as expected its flux is highest in the pore center. In the lower part, where it is a counter-ion, it continues moving downwards, but near the wall. The Na^+ flux is the mirror image of the Glu^- flux. Na^+ enters from the lower compartment into the lower half of the nanopore, and

being a co-ion moves upwards largely in the pore center. Upon entering into the upper half Na^+ continues moving upwards, but near the wall.

The ion fluxes are very different if the bias is regular. Both ion fluxes entering the nanopore as counter-ions are much larger than those if the bias is reverse. The resulting current is their sum because one is a cation and another an anion, but move in the opposite direction. Moreover, their radial profiles complement each other (they are both counter-ions and co-ions depending on where they are within the nanopore). The combined excess ion flux is thus fairly uniform radially throughout the nanopore. The fluxes of ions that enter the nanopore as co-ions are very small and can be ignored. Finally, it should be noted that short bipolar nanopores are not selective. The current is carried by both cations and anions as has also been demonstrated in long nanopores [18]. To summarize, bipolar nanopores rectify because with reverse bias both main contributors to the ion flux start as co-ions in the corresponding half of the nanopore and are very small. Those entering as counter-ions do not go through the nanopore. In contrast with regular bias the flux is carried by ions entering as counter-ions, which are much greater.

Acknowledgments

This work is made possible by the grant support to M.I.G from the Natural Sciences and Engineering Research Council of Canada (Grant No 24776).

References

[1] B. Hille, Ionic Channels of Excitable Membranes, Sinauer Associates Inc., Sunderland, 2001.
[2] J.B. Sorensen, Conflicting views on the membrane fusion machinery and the fusion pore, Annu. Rev. Cell Dev. Biol. 25 (2009) 513–537.
[3] L.J. Breckenridge, W. Almers, Currents through the fusion pore that forms during exocytosis of a secretory vesicle, Nature 328 (1987) 814–817.
[4] M.I. Glavinović, J.M. Trifaró, Change of quantal size and parameters of release with stimulation in bovine chromaffin cells, Pflugers Arch. — Eur. J. Physiol. 443 (2002) 584–594, http://dx.doi.org/10.1007/s00424-001-0732-6.
[5] X. Wang, Y. Li, K.L. Engisch, S.T. Nakanishi, S.E. Dodson, G.W. Miller, T.C. Cope, M.J. Pinter, M.M. Rich, Activity-dependent presynaptic regulation of quantal size at the mammalian neuromuscular junction in vivo, J. Neurosci. 25 (2005) 343–351, http://dx.doi.org/10.1523/JNEUROSCI.3252-04.2005.
[6] D.P. Hoogerheide, Stochastic Processes in Solid State Nanopores, 2010. (PhD Thesis, Harvard).
[7] J. Li, M. Gershow, D. Stein, E. Brandin, J.A. Golovchenko, DNA molecules and configurations in a solid-state nanopore microscope, Nat. Mater. 2 (2003) 611–615.
[8] A. Plecis, R.B. Schoch, P. Renaud, Ion transport phenomena in nanofluidics: experimental and theoretical study of the exclusion–enrichment effect on a chi, Nano Lett. 5 (2005) 1147–1155.
[9] C. Wei, A.J. Bard, S.W. Feldberg, Current rectification at quartz nanopipet electrodes, Anal. Chem. 69 (1997) 4627–4633.
[10] M.A.M. Gijs, Will fluidic electronics take off? Nat. Nanotechnol. 2 (2007) 268–270.
[11] J.H. Han, K. Kim, H. Kim, T. Chung, Ionic circuits cased on polyelectrolyte diodes on a microchip, Angew. Chem. Int. Ed. 48 (2009) 3830–3833.
[12] M. Ali, S. Mafe, P. Ramirez, R. Neumann, W. Ensinger, Logic gates using nanofluidic diodes based on conical nanopores functionalized with polyprotic acid chains, Langmuir 25 (2009) 11993–11997.
[13] K. Tybrandt, K.C. Larsson, A. Richter-Dahlfors, M. Berggren, Ion bipolar junction transistor, Proc. Natl. Acad. Sci. U. S. A. 107 (2010) 9929–9932.
[14] J.T. Santini, M.J. Cima, R. Langer, A controlled-release microchip, Nature 397 (1999) 335–338.
[15] I. Vlassiouk, Z. Siwy, Nanofluidic diode, Nano Lett. 7 (2007) 552–556.
[16] L.J. Cheng, L.J. Guo, Ionic current rectification, breakdown, and switching in heterogeneous oxide nanofluidic devices, ACS Nano 3 (2009) 575–584.
[17] R. Yan, W. Liang, R. Fan, P. Yang, Nanofluidic diodes based on nanotube heterojunctions, Nano Lett. 9 (2009) 3820–3825.
[18] I. Vlassiouk, S. Smirnov, Z. Siwy, Ionic selectivity of single nanochannels, Nano Lett. 8 (2008) 1978–1985.
[19] J.O.M. Bockris, A.K.N. Reddy, Modern Electrochemistry, Plenum Publ, New York, 1976.
[20] A.F. Grodzinsky, Fields, Forces and Flows in Biological Systems, Garland Science, Taylor & Francis Group, London and New York, 2011.
[21] S.G.A. McLaughlin, G. Szabo, G. Eisenman, Divalent ions and the surface potential of charged phospholipid membranes, J. Gen. Physiol. 58 (1971) 667–687.
[22] B. Hille, A.M. Woodhull, B.I. Shapiro, Negative surface charge near sodium channels of nerve: divalent ions, monovalent ions, and pH, Philos. Trans. R. Soc. Lond. B 270 (1975) 301–318.
[23] L.G. Longsworth, Diffusion measurements at 25 °C, of aqueous solutions of amino acids, peptides and sugars, J. Am. Chem. Soc. 75 (1953) 5705–5709.
[24] S.M. Cory, Y. Liu, M.I. Glavinović, Interfacial interactions of glutamate, water and ions with carbon nanopore evaluated by molecular dynamics simulations, Biochim. Biophys. Acta 1768 (2007) 2319–2341.
[25] X. Han, M.B. Jackson, Structural transitions in the synaptic SNARE complex during Ca^{2+}-triggered exocytosis, J. Cell Biol. 172 (2006) 281–293.
[26] P.R. Maycox, T. Deckwerth, J.W. Hell, R. Jahn, Glutamate uptake by brain synaptic vesicles. Energy dependence of transport and functional reconstitution in proteoliposomes, J. Biol. Chem. 263 (1988) 15423–15428.
[27] F.H.J. van der Heyden, D.J. Bonthuis, D. Stein, C. Meyer, C. Dekker, Electrokinetic energy conversion efficiency in nanofluidic channels, Nano Lett. 6 (2006) 2232–2237.
[28] J.D. Machado, M. Camacho, J. Alvarez, R. Borges, On the role of intravesicular calcium in the motion and exocytosis of secretory organelles, Commun. Integr. Biol. 2 (2009) 71–73.
[29] S.H. Behrens, M. Borkovec, Exact Poisson–Boltzmann solution for the interaction of dissimilar charge-regulating surfaces, Phys. Rev. E 60 (1999) 7040–7048.
[30] D. Stein, M. Kruithof, C. Dekker, Surface-charge-governed ion transport in nanofluidic channels, Phys. Rev. Lett. 93 (1-4) (2004) 035901.
[31] I. Vlassiouk, S. Smirnov, Z. Siwy, Nanofluidic ionic diodes. Comparison of analytical and numerical solutions, ACS Nano 2 (2008) 1589–1602.
[32] J.F. Pietschmann, M.T. Wolfram, M. Burger, C. Trautmann, G. Nguyen, M. Pevarnik, V. Bayer, Z. Siwy, Rectification properties of conically shaped nanopores: consequences of miniaturization, Phys. Chem. Chem. Phys. 15 (2013) 16917–16926.
[33] G. Nguyen, I. Vlassiouk, Z.S. Siwy, Comparison of bipolar and unipolar ionic diodes, Nanotechnology 21 (2010) 1–8.